Microchannels and Minichannels - 2004
June 17-19, 2004, Rochester, New York, USA

ICMM2004 – xxxx

DIRECT COMPARISON BETWEEN A VARIETY OF MICROCHANNELS PART 2: EXPERIMENTAL DESCRIPTION AND FLOW FRICTION MEASUREMENT

Cormac Eason[1], Tara Dalton[1], Cian O'Mathúna[2], Mark Davies[1], Orla Slattery[2]
[1]Stokes Research Institute, University of Limerick, Co. Limerick, Ireland, ceason@skynet.ie
[2]NMRC, University College Cork, Cork, Ireland, cian.omathuna@nmrc.ie

ABSTRACT

Part 1 of this paper (Eason et al 2004) investigates the manufacturing of a variety of microchannels, produced by wet and dry etching in silicon, as well as precision mechanical sawing in silicon and thermoset plastic. This paper describes the experimental equipment and methods used to measure the pressure flow characteristics of the manufactured channels.

A custom designed test system has been built in order to test each sample using the same inlet and outlet manifolds, pressure tappings, pumping system and instrumentation. The pressure drop across each set of channels was measured using an inductive pressure transducer. The mass flow rate through the system is measured by weighing the flow from the system in a given time.

The measured pressure flow behaviour was compared with theoretical values as calculated from macro scale theory. Channel dimensions used for this calculation are as measured in part 1 of this paper. Error analysis was then carried out in order to determine the overall accuracy of the experimental work and determine whether any deviation from theoretical values is of experimental significance. This step is essential in any attempt to determine whether microchannel flows are indeed different to macro scale flows in a fundamental way.

The deep reactive ion etched (DRIE) channels show the most significant lack of correlation with theoretical predictions. Compensation must be introduced to deal with the difference in cross section between the perfectly rectangular channels used for the theoretical prediction and the actual cross section of the channels.

NOMENCLATURE

Symbol	Description	Unit
A	Cross Sectional Area of a Channel	m^2
$A1$	Cross Sectional Area for Contraction Loss	m^2
$A2$	Cross Sectional Area for Contraction Loss	m^2
C	Pressure Transducer Calibration Const.	Pa/V
D_h	Hydraulic Diameter	m
K_L	Loss Coefficient	No Unit
L	Length of Channel	m
P_L	Pressure drop along channel	Pa
Re	Reynolds Number	No Unit
T_{bp}	Fluid temperature at bypass outlet	K
T_o	Fluid outlet temperature	K
T_{res}	Reservoir temperature	K
V_{bp}	Bypass Valve Setting	rev
V_m	Master Valve Setting	rev
V_P	Pressure transducer voltage	V
f	Friction factor	No Unit
m	Liquid Mass flowing through system	g
$\dot{m}$	Mass Flow Rate	g/s
n	Pump RPM	rev/min
t	Time taken for fluid to be collected	s
u	Mean velocity of fluid in test channel	m/s
w_m	Uncertainty in Mass Measurement	g
$w_{\dot{m}}$	Uncertainty in Mass Flow	g/s
w_t	Uncertainty in Time Measurement	g/s
	Greek Symbols	
μ	Viscosity of Fluid	Pa s
ρ	Density of Fluid	kg/m^3

INTRODUCTION

A considerable body of research has been performed on fluid flow in microchannels with inconclusive results.

Variation in measured friction factors from 0.5 to 2.5 times predicted theoretical values have been reported by 6 separate experimenters (Paputski, 1999), Judy, (2002) references papers measuring friction factors above and below theoretical values, but finds no experimentally significant deviation from expected values at all. Wu (2003) and Gao (2002) also report experimental values close to theoretical predictions. This paper aims to produce reliable data to add to the body of information already available in the area of pressure drop through microchannels.

The manufacturing methods used were developed with the NMRC and made use of precision sawing in plastic, silicon and glass, Deep Reactive Ion Etching (DRIE) and KOH Etching. The manufacturing processes and measurement of the dimensions of the channels are detailed in part one of this paper (Eason et al, 2004).

Fundamental to any study to be performed on microchannels is the equipment used to test them and measure their behaviour. A system where the channels are covered over by a glass slide, clamped in place to create a seal was designed in order to allow easy dismantling and cleaning of the system as well as providing visual access to the channels. This has the advantage that problems such as air bubbles and blockages and other unexpected behaviour can be seen without dismantling the system.

EXPERIMENTAL DESCRIPTION

The microchannel test apparatus comprises of a gear pump, a fluid reservoir, tubing to join the microchannel modular block to the pump and two micrometer adjustable needle valves to control flow to the microchannel array.

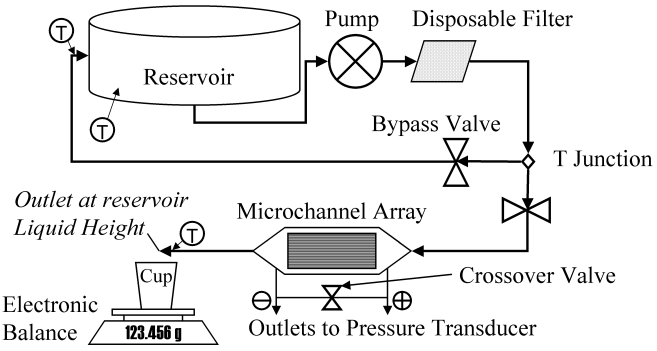

Figure 1: Schematic of the microchannel characterization equipment. The encircled 'T's indicate where thermocouples are fitted to the system.

The reservoir has a diameter of 270mm. The reason such a large diameter was chosen is to prevent significant changes in the liquid height over the duration of an experiment. In addition, the reservoir is covered to prevent contamination from settling into the water from the air.

The pump motor is a feedback controlled Tuthill V2DC unit that will deliver speeds from 60 to 3600 rpm. The motor is magnetically coupled to a Tuthill DDS.19 gear pump. This pump can supply pressures of up to 1.72MPa at a temperature of 177°C. The pump supplies a flow rate of 0.19ml/revolution, assuming zero slip in the pump. The liquid used for all tests described here is distilled and deionised water.

The micrometer adjustable valves have been named the master and bypass valves and are fitted as in Figure 1 with the master valve in series with the pump and channels and the bypass valve controlling flow through a tube that bypasses the microchannel block, returning directly to the reservoir. Using this system, steady flow rates much lower than the pump delivers directly can be supplied to the channels. Closing the bypass valve diverts all flow through the channels.

K-Type thermocouple probes are used to measure the temperature of the reservoir, bypass circuit and the temperature of the exiting fluid. The purpose of these thermocouples is to investigate whether there is any significant temperature change in the system over the course of the experiment. Viscous heating has been calculated to be negligible for the channels and flow rates tested. The pump however, does add some heat to the system.

The pressure drop across the channels is measured using a Validyne DP15 differential pressure transducer. This transducer measures the change in inductance caused by the deflection of a diaphragm due to the pressure difference between its two sides. By using diaphragms of varying thicknesses, pressure ranges from a full scale of 860 ±2Pa to a full scale of 22,000 ±55MPa can be measured. For the experiments described here a diaphragm with pressure range from 0 to 14kPa was used.

By adjusting the pump speed and valve settings, the system is capable of supplying steady flow ranging from a maximum of 10.3g/s to less than 0.015g/s at pressures up to 1.72Mpa. This mass flow range is beyond the capabilities of any in line mass flow measurement device the authors are aware of. For this reason weighing the fluid pumped through the system over a timed interval was the method used to take mass flow readings.

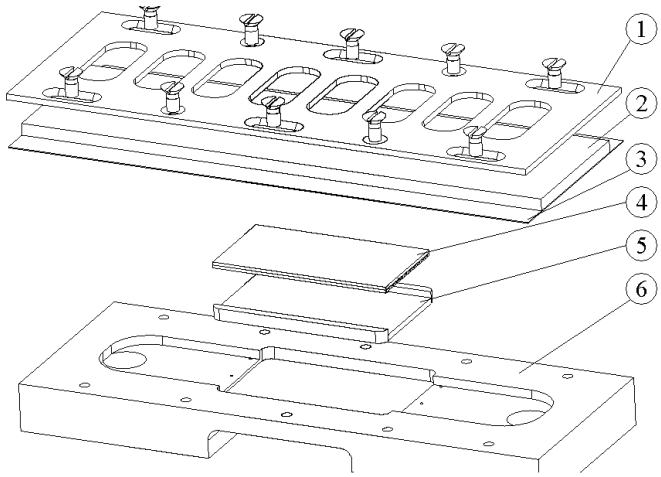

Figure 2: Layout of the Microchannel Tester

A digital balance and stopwatch are used for the mass and time measurements. All measurement durations apart from the maximum flow rates through the trapezoidal channels were over a minimum of 60 seconds.

Measurements of evaporation from a collection cup over 4 days predict that approximately 1.4mg of water will be lost over a minute. This is negligible compared to the ±1 drop (0.08g) uncertainty already associated with the mass measurement. All mass measurements are of 3g or more.

The time over which the mass is collected is measured using a quartz stopwatch accurate to ±5 seconds/month. Operator error in the use of this device is taken to be ±0.5 seconds.

As shown in Figure 2, the fluid is sealed into the block by gasket paper (3) compressed by a glass slide (2), which is clamped in position by a cover plate (1). The 16×30mm sample (4) fits into the shim (5), which then fits into a recess in the manifold block (6). Because the samples are available in a variety of thicknesses, several shims have been made with different depth grooves. The result of this is that all the channel samples, when fitted in their corresponding shims, occupy the same volume. Since the only change in the flow system from sample to sample is the size of the channels being tested, the effects of different manifolds, pressure tapping locations and thermocouple locations as experienced in systems where each set of channels is machined with its own manifold are eliminated.

APPARATUS CALIBRATION

Prior to performing any experiments, the test system must be shown to produce repeatable data, as well as producing steady flow. The steadiness of the gear pump motor was confirmed by using an optical digital tachometer to measure the actual pump speed in order that it could be compared to the speed indicated by the pump. All results from this test measured the pump speed to be accurate to less than ±1 rpm regardless of load or speed. This improves in the manufacturer's claim of ±9rpm accuracy. Repeated flow tests at the same pump settings and different time intervals also show the pump output to be steady.

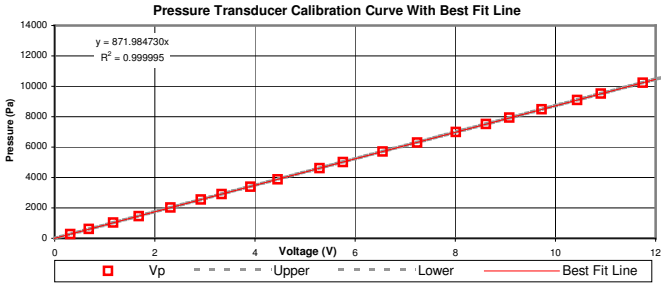

Figure 3: Calibration Curve for Pressure Transducer with upper and lower uncertainty envelope. Note correlation coefficient for best fit line is almost 1. A correlation coefficient of 1 means a perfect correlation.

The pressure transducer was calibrated using columns of water. The Voltmeter is a digital auto ranging model made by Fluke. It reads to 0.1mV from 2 to 12V and to 0.01mV below 2V. Because of the static nature of the loading on the transducer during calibration, readings were stable to ±0.5mV. During experimental readings, the voltmeter is stable to ±50mV (See Table 3). The overall error for pressure readings during calibration of the transducer, accounting for errors in reading the water level, curve fitting error and Voltmeter fluctuation is ±42.5 Pa or 0.3% of full scale deflection.

The point data recorded during the calibration fitted almost perfectly to a straight line through the origin (Correlation coefficient r^2=0.999995), allowing the slope of the best fit line to be confidently used to convert the voltage reading produced by the transducer to a pressure reading in Pascals. This constant, C = 871.98 Pa/V and the curve and data points from which it is generated are shown in Figure 3.

K-Type thermocouples were used for all readings. They were calibrated in a temperature controlled water bath to read accurately to ±0.1K. The weighing scales used is a Sartorius BL150S digital balance, factory calibrated to ±0.001g, that can measure masses of up to 150g.

EXPERIMENTAL PROCEDURE

The experimental procedure begins with ensuring the apparatus is set up correctly. The electronic balance is leveled and the outlet pipe from the microchannel test section is adjusted to the same height as the fluid in the reservoir. The reservoir height is indicated by tube that siphons water from the reservoir and is held beside the outlet from the channels.

Once the initial setup is complete, the master valve is opened and the pump turned on at low speed. Opening the crossover valve between the positive and negative sides of the pressure transducer and running the pump at full speed removes any bubbles visible in the system. The crossover valve is opened to eliminate the possibility that the pressure transducer is overloaded.

To record a data point on the pressure flow curve, the pump speed and master/bypass valves are adjusted until a target pressure drop is indicated by the voltmeter. The system is left to settle for about a minute and then the scales is zeroed and a timed mass flow reading begins. Each reading is repeated at least twice and usually three or more times for a given pressure setting. The flow through the system is then readjusted to give a new pressure drop and the process is repeated again. At least two complete flow curves were recorded for each channel type.

CALCULATIONS

Table 1: Raw Data Measured from the Test System

Description	Symbol	Unit
Fluid temperature at bypass outlet	T_{bp}	°C
Fluid outlet temperature	T_o	°C
Reservoir temperature	T_{res}	°C
Bypass Valve Setting	V_{bp}	rev
Master Valve Setting	V_m	rev
Pressure transducer voltage	V_P	V
Mass of Liquid flowing through system	m	g
Pump RPM	n	rev/min
Time taken for fluid to be collected	t	s

The quantities listed in Table 1 are measured directly from the test system. A Program written in Matlab was then

used to convert this raw data into pressure and mass flow results. A second program has also been written which calculates the theoretical pressure drop in the channels based on their shape and aspect ratio. Further work will allow the same program to predict the Nusselt number. The data used for these calculations was intended for large size channels and can be found in Çengel (1998) and Rohsenow (1985). The channel dimensions are the averaged dimensions of the channels in each sample as measured using a Scanning Electron Microscope (SEM) (Eason et al, 2004).

Since the pressure tappings do not coincide with the channel entrance and exit, the pressure drop measured by the experimental apparatus includes the contraction and expansion losses at the entrance and exit of the channels and the friction losses experienced by the fluid as it travels through the manifold from the pressure tappings to each end of the channels.

Darcy's Equation is used to calculate the pressure drop for fluid flowing in the channels and the inlet and outlet manifolds. If the friction factor f is set equal to $16/Re$ this gives the correlation for laminar flow. It should be noted that when μ, ρ and D_h remain constant, P_L is directly proportional to the mass flow rate $\dot{m}$ for laminar flow. Data measured from the system confirms this proportionality.

To account for the contraction and expansion losses at the entrance and exit of the channels, a similar equation is used. This is shown in Equation (1) (Howatson et al, 1995).

$$P_L = K_L \frac{\rho u^2}{2} \quad \textbf{(1)}$$

In Equation (1) P_L is proportional to $\dot{m}^2$. This is why the result plots are not perfectly linear. It should be noted that the contraction, expansion and manifold friction losses form less than 8.7% of the total pressure drop for even the highest Reynolds numbers used here, and are less than 1% at lower Re values. The value of K_L changes depending on the area ratio between the channel and the manifold. The manifold area divided by the number of channels in the sample is used as the $A1$ for the inlet and $A2$ for the outlet calculation. To calculate K_L for inlet loss the Matlab program interpolates linearly between the values given in Table 2.

Table 2: Loss Coefficient Vs. Area Contraction Ratio (Howatson et al 1995).

$A2/A1$	0	0.1	0.2	0.4	0.6	0.8	0.9	1
K_L	0.5	0.37	0.35	0.27	0.17	0.06	0.02	0

K_L for expansion losses is found using Equation (2).

$$K_L = \left(1 - \frac{A1}{A2}\right)^2 \quad \textbf{(2)}$$

Once the program has been given the correct channel and manifold dimensions, it calculates the pressure drop, as well as the Reynolds number, Nusselt number and friction factor for the channels. All these calculations are based on existing correlations for large size channels.

UNCERTAINTY ANALYSIS

Table 3 shows a list of all the information recorded from the test system during each experiment as well as the manufacturer's stated uncertainty for each measurement and the actual experimental uncertainty for each measurement as it performed in the experimental apparatus.

Table 3: Experimental Uncertainty. Values in bold indicate where the experimental uncertainty and the stated accuracy of a particular measurement differ.

Measurement	Stated Accuracy	Experimental Uncertainty
Temperature	±0.1°C	±0.1°C
Voltage (Fluke Voltmeter)	±0.0001V	**±0.05V**
Mass	±0.001g	**±0.08g**
Time	±0.01s	**±0.5s**
Master/Bypass Valves	$\pm^1/_{50}$th Turn	$\pm^1/_{50}$th Turn
Pump RPM	±9 rpm	**±1 rpm**

In order to calculate the experimental uncertainty in the mass flow, the formula in Equation (3) was used (Holman, 1989).

$$w_{\dot{m}} = \left[\left(\frac{\partial \dot{m}}{\partial t} w_t \right)^2 + \left(\frac{\partial \dot{m}}{\partial m} w_m \right)^2 \right]^{\frac{1}{2}} \quad \textbf{(3)}$$

This calculation is performed on every mass flow measurement. In order to produce a single mass flow figure to describe the accuracy of a flow curve, the uncertainty figures were averaged and their sample standard deviation found. A 95% confidence interval (CI) for the mass flow uncertainty is found by adding 1.65 times the standard deviation to the average uncertainty. A standard 95% CI is the average value ±2 Standard Deviations, but since all the lower values of the uncertainty indicate greater than average accuracy, 95% of all results will be contained in the range from zero to the average plus 1.65 standard deviations. The calculated uncertainties are shown in error bars on the flow curves plotted in the results section.

Uncertainty in pressure measurement was calculated by adding the calibration error for the transducer (±42.5 Pa) to the extra uncertainty caused by the increase in fluctuation in the voltmeter as a result of performing measurements on a dynamic system. The resulting error is ±86.7 Pa. This is shown on the error bars in the result plots. It is a very small error in comparison with the pressures being measured (0.63% of Full Scale Deflection), so the y error bars can only be seen clearly in Figure 9.

RESULTS

Five different types of channels were tested. Detail on how the channels were measured can be seen in Part 1 of this paper (Eason et al, 2004).

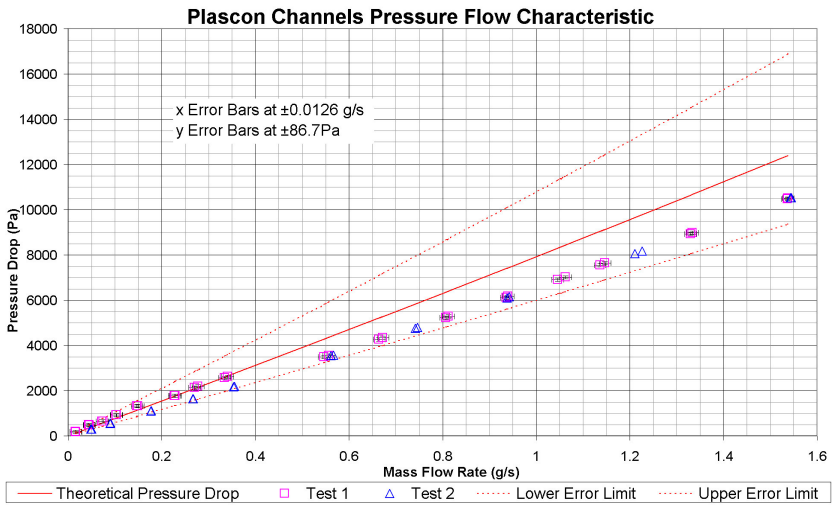

Figure 4: Pressure flow curve for diced Plascon Channels 0.203W×0.382H (mm). Max Re = 240.

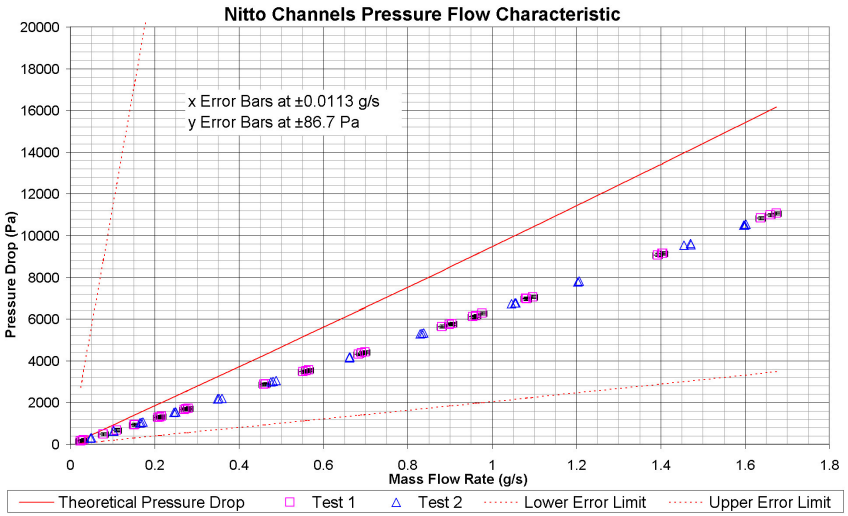

Figure 5: Pressure flow curve for diced nitto channels 0.202W×0.344H (mm). Max Re = 279.

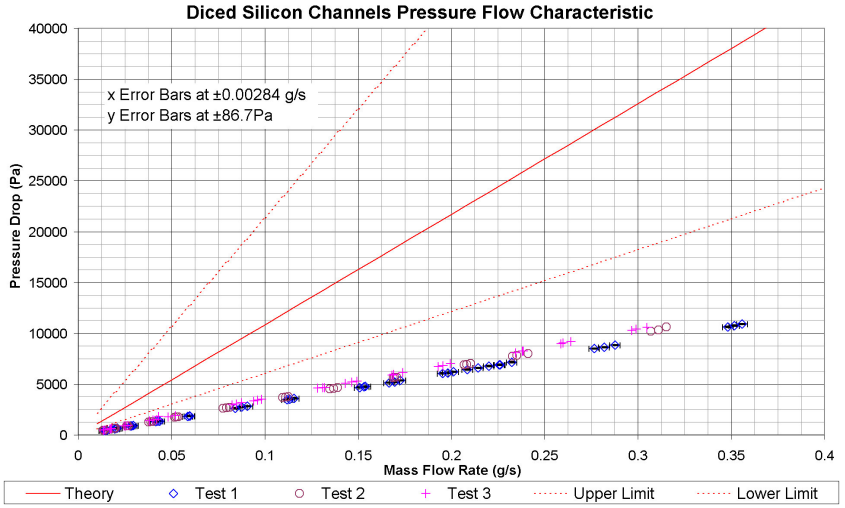

Figure 6: Pressure flow curve for diced silicon 0.052W×0.423H. Max Re = 20.5.

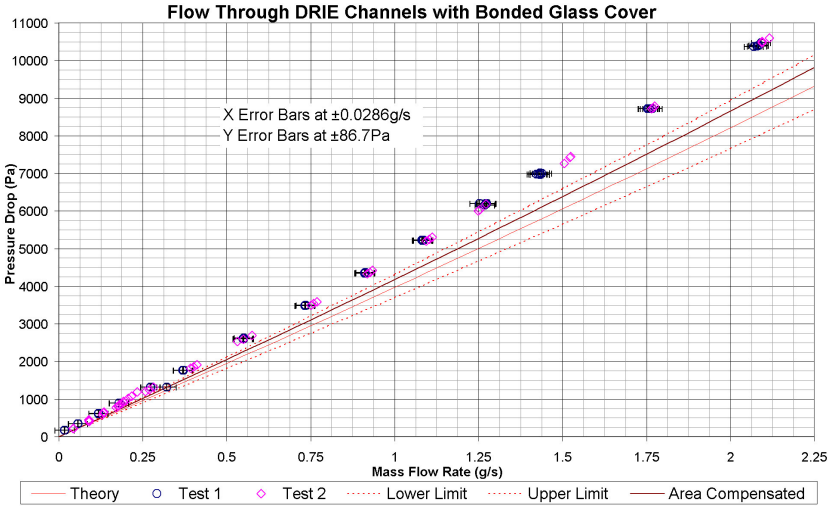

Figure 7: Pressure flow curve for DRIE channels0.304W×0.332H (mm). Max Re = 300

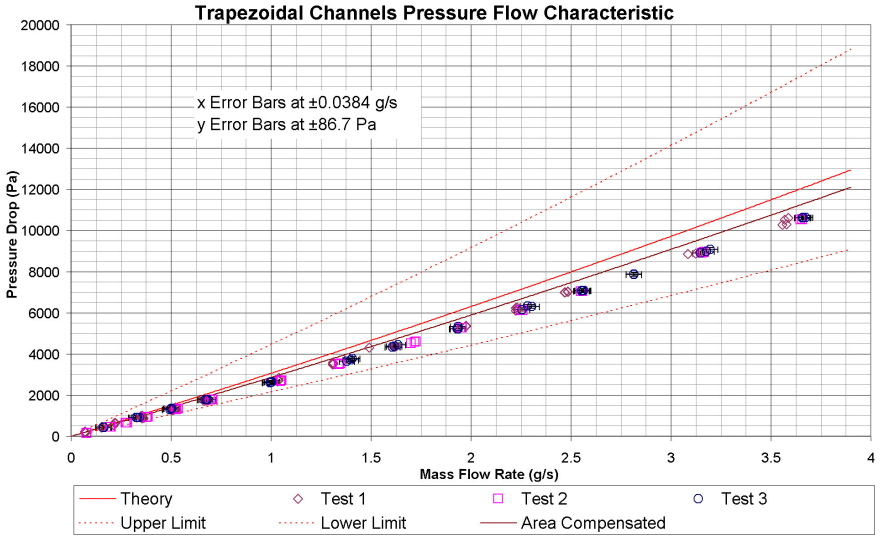

Figure 8: Pressure flow curve for wet etched channels 0.577W×0.413H (mm). Max Re = 417.

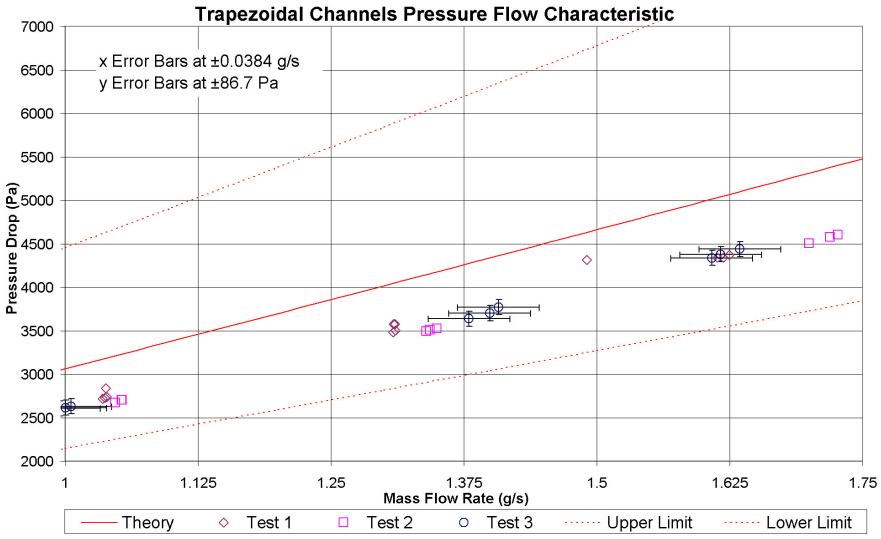

Figure 9: Zoomed area on Figure 8. The small range in the uncertainty of the experimental readings can be seen clearly here.

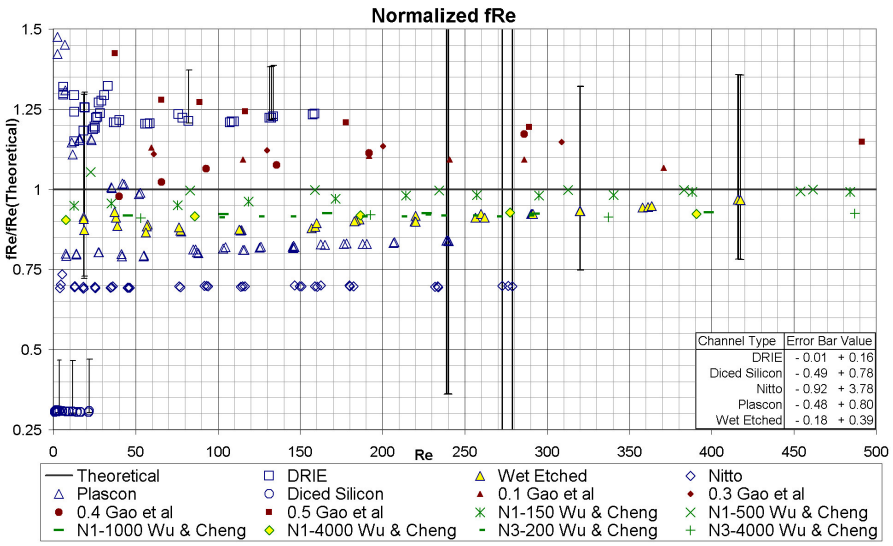

Figure 10: Normalized friction factors for the channels tested compared with normalized data from other researchers.

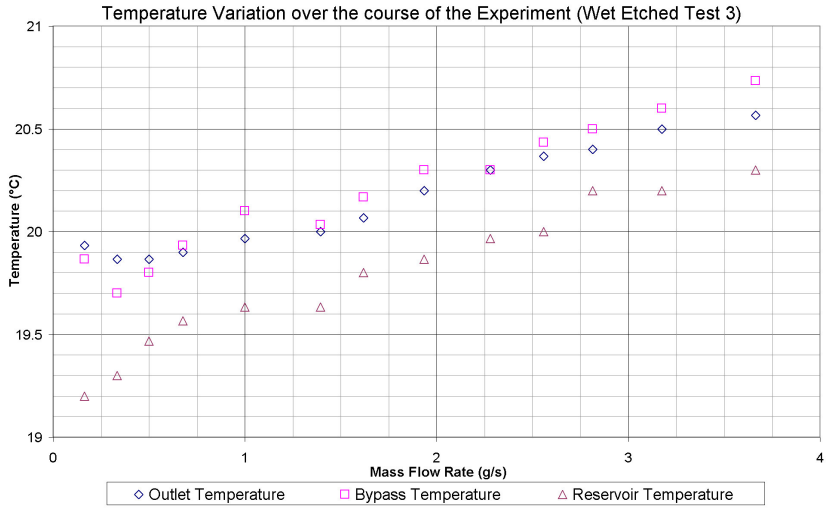

Figure 11: Temperature variation in the fluid in the channel outlet, bypass outlet and reservoir over the course of Test 3 run on the wet etched (Trapezoidal) channels. Room temperature was 19.6°C for this experiment.

Table 4: Scanning Electron Microscope (SEM) Measurements of 5 Sets of Microchannels. (95% Confidence Interval (CI) = Average Value ± 2×Sample Standard Deviation)

	Wet Etched	Diced Silicon	DRIE	Nitto Plastic	Plascon Plastic
SEM Data (Measured/Available)	22/22	20/61	22/22	22/22	22/22
Average CSA (mm^2)	0.1263	0.0218	0.1008	0.0728	0.0777
Standard Deviation (mm^2)	0.00525	0.00223	0.00152	0.01791	0.01040
% Deviation (95% CI)	8.31%	20.47%	3.01%	49.17%	26.78%

Table 5: Comparison between SEM measurement of individual channels and CAD model created from points taken from a SEM photograph of the same channel.

	Wet Etched	Diced Silicon	DRIE	Nitto Plastic	Plascon Plastic
CSA from SEM (mm^2)	0.126878	0.021827	0.102701	0.077563	0.100015
CSA from CAD Model (mm^2)	0.131198	0.019002	0.100054	0.075792	0.093405
% Change	+3.41%	-12.94%	-2.58%	-2.28%	-6.61%

DISCUSSION

It can be seen from the pressure flow curves in Figure 4 to Figure 9 that all the curves except for those for those recorded for the DRIE and diced silicon channels fall within the error envelope. The pressure flow curves also show that the pressure and flow rate relationship is almost perfectly linear. This result is exactly as expected for laminar flow. The slight non-linearity is as a result of the entrance and exit effects discussed in the Calculations Section.

Part 1 of this paper measures the channels in two ways. The first takes a single vertical and horizontal measurement from each channel, calculates the area of each channel idealized as a rectangle or trapezoid and averages these areas to give an average area for the sample. The second method measures points taken from a SEM photograph of the channel and uses them to build an accurate CAD model of the real channel cross section. The change in the cross sectional area data is copied from Part 1 of this paper (Eason et al, 2004) to Table 5.

The theoretical pressure flow characteristic curve is calculated using a Matlab program treating the channels as perfect rectangles or trapezoids. The error envelope shown with the dashed lines on each side of the theoretical line is found by recalculating the pressure drop for the channels using the maximum and minimum channel sizes as found by adding or subtracting two standard deviations from the mean value. Statistically this gives a 95% probability that all experimental results will fall within this envelope. The error bars on specific points on the graph also show the 95% confidence interval for that particular measurement.

To compensate for the fact that the channels are not perfect rectangles or trapezoids, the actual area of the channels was measured from digitized SEM photographs using the technique described in Part 1 of this paper (Eason et al, 2004).

By substituting the relations $D_h^2 \propto A$ and $u \propto A$ into Darcy's Equation, for laminar flow where $f \propto 1/Re$, the relationship between the theoretical pressure drop, the area compensated pressure drop and the theoretical and measured cross sectional areas is as shown in Equation (4).

$$\frac{P_{L1}}{P_{L2}} = \frac{A_2^{\,2}}{A_1^{\,2}} \qquad \textbf{(4)}$$

Applying this correction to the theoretical calculations improves the correlation between the theoretical wet etched and DRIE channel pressure drops and the experimentally measured pressure drops. The recalculated theoretical curves for the DRIE and wet etched channels are shown in the area compensated curves in Figure 7 and Figure 8.

This compensation does not improve the results from the other three channels. This means that some other more significant effect must be causing the other channels to deviate. For the plastic channels, the gap between the glass cover and the tops of the channels is the most likely cause of the experimental deviation. This is mostly filled by the SU8 photoresist used to bond the glass over the channels, but the slight warping in the plastic channels prevented a complete bond from forming. These are still within the uncertainty envelope calculated for them from theory, though they are likely to be better centered on the theoretical curve if the glass bond was complete.

The error in the diced silicon channels is most likely due to leakage occurring around the silicon sample in the test system. This is more likely to occur than with the other samples because the diced channels were not glass covered. Fluid leaking over the channels will increase the cross section available for flow and in doing so give a far lower pressure drop for a given flow rate. The flow rates for the diced silicon channels are between a quarter and a tenth of the flows through the other channels, so the same amount of leakage over the channels will have a more significant effect on the results than it would have for the other channels tested.

The error in the DRIE channels is more difficult to explain. The DRIE channels are by far the most consistent in terms of their shape and size compared to any of the other channels tested. The results seem to indicate that the channels may be smaller than the SEM data indicates. Since the cross section is measured only at the plane of the

entrance of the channel, there's a possibility that the channel cross section drops further down the channels. Area compensation improves the theoretical results, just failing to bring the experimental pressure flow curve for the DRIE channels within the theoretical uncertainty envelope. Fully developed flow is assumed for theoretical calculations so calculations may need to be modified to account for developing flow.

In order to compare the results measured for these experiments with results measured by other researchers, the friction factor times *Re*, as measured from the experimental work, were divided by the theoretical *fRe* values calculated for each channel shape using data from Çengel (1998) and Rohsenow (1985). Figure 10 is a plot of the normalized *fRe* measured from the experiments described here, as well as results from papers by Gao et al (2002) and Wu and Cheng (2003). The closer each y-value is to 1, the better it correlates with accepted macro scale flow theory.

The paper by Wu and Cheng tests a variety of triangular and trapezoidal microchannels. Results from the wet etched channels tested in this paper correlate well with Wu and Cheng's results, as well as being within 15% of theory. The N1-4000 channel has the closest hydraulic diameter to the wet etched channel tested here. The paper by Gao et al measures friction factors from channels 25mm wide and of heights varying from 0.1 to 1mm. All these have significantly higher aspect ratios than the rectangular channels tested however. All the rectangular channel data apart from that from the diced silicon channels correlates quite well with the theoretical values.

Figure 11 shows a plot of the variation in the temperature of the fluid for Test 3 on the wet etched channels. All recorded temperatures were similar for all experiments. Temperature variation is almost entirely due to heating from the pump. This can be seen in the bypass fluid temperature, which is slightly higher than the temperature of the fluid that has passed through the channels. The bypass is closer to the pump than the outlet from the channels and therefore has less time to lose the heat to the ambient air.

The stepping in the temperature of the reservoir is due to the water collected for weighing being poured back into the reservoir periodically. The system is left to stabilize after this has been done in order to ensure that the increase in the height of the reservoir does not affect the system. Height changes are a maximum of 8mm (7.8Pa), so this change should not affect flow in the system significantly.

CONCLUSIONS

The general flow behavior correlates very well with standard macro scale laminar flow theory.

The 95% confidence interval for the results perfectly encompasses 3 of the 5 channels tested.

The test on the diced silicon channels shows clear evidence of leakage over the channel sample. This will be improved in subsequent experiments by increasing the clamping pressure over the channels and using a more compliant gasket material.

The DRIE channel results are the only measurements that initially seem to deviate in an experimentally significant way from the theoretical calculations. However, when the flow curve is modified to compensate for the difference in area between a perfect rectangular channel as modeled by the theoretical prediction software and the actual cross sectional area of the channel, the theoretical flow curve shifts far closer to the behaviour measured during the experiment.

The *fRe* values calculated from the system correlate reasonably well with theory and the work of other researchers. The 95% CI on these measurements indicates a high level of error in the calculation of the *fRe* values.

The heating effect of the pump is not enough to change the properties of the test fluid significantly over the course of an experiment. Cooling loops will be added to the system for thermal measurements to regulate coolant temperature.

The microchannels tested here do not show experimentally significant differences in behavior compared to larger channels.

ACKNOWLEDGMENTS

Many thanks to Paddy O'Regan for his machining work on the custom designed parts of the test system.

REFERENCES

1. Çengel, Yunus A.; Heat Transfer, a Practical Approach; *McGraw Hill 1998, Page 380.*
2. Eason, Cormac; Dalton, Tara; O'Mathuna, Cian; Slattery, Orla; Davies, Mark; Direct Comparison Between a Variety of Microchannels – Part 1: Channel Manufacture and Measurement, *Second international conference on micro and mini channels, 2004.*
3. Gao, Puzhen; Le Person, Stéphane; Favre-Marinet, Michel; Scale Effects on Hydrodynamics and Heat Transfer in Two-dimensional Mini and Microchannels; *International Journal of Thermal Sciences 41 (2002) 1017-1027.*
4. Holman J.P.; Gajda Jnr., W.J.; Experimental Methods for Engineers, 5th Edition; McGraw Hill (1989), Pages 41-42.
5. Howatson, A. M.; Lund, P. G.; Todd, J. D.; Engineering Tables and Data, Second Edition, *Chapman and Hall (1995)*
6. Judy, J.; Maynes, D.; Webb, B. W.; Characterization of frictional pressure drop for liquid flows through microchannels, *International Journal of heat and mass transfer 45 (2002) 3477-3489*
7. Paputski, Ian; Gale, Bruce K.; Mohanty, Swomitra; Ameel, Tim A. and Frazier, A. Bruno; Effects of Rectangular Microchannel Aspect Ratio on Laminar Friction Constant, *Proceedings of SPIE - The International Society for Optical Engineering, Proceedings of the 1999 Microfluidic Devices and Systems II, Santa Clara, vol 3877, 1999, pp. 147-158.*
8. Rohsenow, W. M.; Hartnett, J. P. and Ganic, E. N.; Handbook of Heat Transfer Fundamentals, Second Edition, *McGraw Hill (1985), pages7-91, 7-118.*
9. Wu, H. Y.; Cheng, Ping; Friction Factors in Smooth Trapezoidal Silicon Microchannels with Different Aspect Ratios; *International Journal of Heat and Mass Transfer 46 (2003) 2519-2525.*